Supplemental Tables

Table S1. Patients. Related to Figures 1 to 8.

	Spatial reference memory task			Hybrid spatial navigation–episodic memory task		
Patient	**Index**	**Session**	**# Trials**	**Index**	**Session**	**# Trials**
1				TH_001	0	21
					2	39
2	OF_001	OF_001a	39	TH_002	0	32
		OF_001b	78		1	32
3	OF_002	OF_002	34	TH_003	1	40
					2	28
4	OF_003	OF_003a	167	TH_004	0	40
		OF_003b	162		1	40
5	OF_004	OF_004a	166	TH_005	0	40
		OF_004b	162		1	40
6	OF_005	OF_005	54	TH_006	0	40
					1	40
7	OF_006	OF_006	98	TH_007	0	24
8	OF_007	OF_007	36			
9	OF_008	OF_008	67			
10	OF_009	OF_009	162	TH_008	0	32
					1	24
11	OF_010	OF_010	102			
12	OF_011	OF_011	54	TH_009	0	40
13	OF_012	OF_012	102	TH_010	0	40
					1	40
14	OF_013	OF_013a	167	TH_011	0	40
		OF_013b	164			
15	OF_014	OF_014	94	TH_012	0	40

Table S2. Additional characteristics of findings. Related to Figures 2, 3, 4, 5, 6, 8, S5, S6, and S8.

Figure	Additional characteristics of findings for illustrative purposes
2A, middle	ANOVA statistics associated with the tuning curve: $F(11, 29506) = 6.706$, $p < 0.001$. Difference between maximum and minimum firing rate = 0.946 Hz.
2B, middle	ANOVA statistics associated with the tuning curve: $F(11, 20896) = 3.016$, $p < 0.001$. Difference between maximum and minimum firing rate = 1.267 Hz.
2C, middle	ANOVA statistics associated with the tuning curve: $F(11, 8033) = 3.839$, $p < 0.001$. Difference between maximum and minimum firing rate = 1.148 Hz.
2D, middle	ANOVA statistics associated with the tuning curve: $F(11, 18459) = 3.600$, $p < 0.001$. Difference between maximum and minimum firing rate = 1.278 Hz.
2E, middle	ANOVA statistics associated with the tuning curve: $F(11, 20896) = 5.639$, $p < 0.001$. Difference between maximum and minimum firing rate = 0.496 Hz.
3F, left	Linear fit (red line): $y = 0.248 * 10^{-3} * x - 0.130$. Difference between maximum and minimum firing rate = 0.915 Hz.
3F, right	Linear fit (red line): $y = -0.147 * 10^{-3} * x + 1.220$. Difference between maximum and minimum firing rate = 0.950 Hz.
3H	Average firing rate within the bearing-distance field: 11.325 Hz; average firing rate outside the bearing-distance field: 8.937 Hz. The difference is 2.388 Hz.
3I	Average firing rate within the bearing-distance field: 1.079 Hz; average firing rate outside the bearing-distance field: 0.495 Hz. The difference is 0.584 Hz.
3J, left	Average firing rate within the bearing-distance field: 8.136 Hz; average firing rate outside the bearing-distance field: 5.754 Hz. The difference is 2.382 Hz.
3J, right	Average firing rate within the bearing-distance field: 3.573 Hz; average firing rate outside the bearing-distance field: 2.817. The difference is 0.756 Hz.
3N, left	Linear fit (red line): $y = 0.871 * x - 0.418$.
3N, right	Linear fit (red line): $y = -2.040 * x + 0.959$.
4A	ANOVA statistics associated with the tuning curve: $F(7, 8037) = 11.729$, $p < 0.001$. Difference between maximum and minimum firing rate = 2.948 Hz.
5B	Average firing rate within the significant time window for preferred objects: 0.602 Hz; average firing rate within the significant time window for unpreferred objects: -0.070 Hz. Paired t test: $t(122) = 4.218$, $p < 0.001$.
5C	Average firing rate within the significant time window for object by egocentric bearing cells: 1.837 Hz; average firing rate within the significant time window for object by non-egocentric-bearing cells: 0.269 Hz. Two-sample t test: $t(121) = 4.275$, $p < 0.001$.
5F	Average firing rate within the significant time window for close objects: 0.291 Hz; average firing rate within the significant time window for far objects: -0.070 Hz. Paired t test: $t(89) = 3.103$, $p = 0.003$.
6C, middle	ANOVA statistics associated with the tuning curve: $F(11, 6401) = 2.031$, $p = 0.022$. Difference between maximum and minimum firing rate = 1.064 Hz.
6D, middle	ANOVA statistics associated with the tuning curve: $F(11, 5739) = 3.096$, $p < 0.001$. Difference between maximum and minimum firing rate = 1.024 Hz.
6E, middle	ANOVA statistics associated with the tuning curve: $F(11, 6537) = 2.492$, $p = 0.004$. Difference between maximum and minimum firing rate = 0.439 Hz.

6F, middle	ANOVA statistics associated with the tuning curve: $F(11, 6588) = 2.218$, $p = 0.011$. Difference between maximum and minimum firing rate = 0.779 Hz.
6G, middle	ANOVA statistics associated with the tuning curve: $F(11, 6588) = 12.111$, $p < 0.001$. Difference between maximum and minimum firing rate = 2.665 Hz.
8B	Average firing rate within the significant time window (successful>unsuccessful) for successful trials: 0.446 Hz; average firing rate within the significant time window (successful>unsuccessful) for unsuccessful trials: 0.135 Hz; paired t test between successful and unsuccessful trials: $t(73) = 2.511$, $p = 0.014$. Average firing rate within the significant time window (successful>0) for successful trials: 0.446 Hz; one-sample t test for successful trials versus 0: $t(73) = 2.099$, $p = 0.039$.
8D	Average firing rate within the significant time window for successful-unsuccessful trials in egocentric bearing cells: 0.311 Hz; average firing rate within the significant time window for successful-unsuccessful trials in non-spatial cells: 0.034 Hz; two-sample t test: $t(651) = 2.674$, $p = 0.008$.
8F	Average firing rate within the significant time window (successful>unsuccessful) for successful trials: 0.295 Hz; average firing rate within the significant time window (successful>unsuccessful) for unsuccessful trials: -0.118 Hz; paired t test: $t(73) = 3.090$, $p = 0.003$. Average firing rate within the significant time window (successful>0) for successful trials: 0.295 Hz; one-sample t test for successful trials versus 0: $t(73) = 2.445$, $p = 0.017$.
8H	Average firing rate within the significant time window for successful-unsuccessful trials in egocentric bearing cells: 0.350 Hz; average firing rate within the significant time window for successful-unsuccessful trials in non-spatial cells: -0.037 Hz; two-sample t test: $t(651) = 3.147$, $p = 0.002$.
S5A	ANOVA statistics associated with the tuning curve: $F(11, 29517) = 23.435$, $p < 0.001$. Difference between maximum and minimum firing rate = 1.540 Hz.
S6A	ANOVA statistics associated with the tuning curve: $F(49, 17045) = 1.799$, $p < 0.001$. Difference between maximum and minimum firing rate = 1.951 Hz.
S6B	ANOVA statistics associated with the tuning curve: $F(39, 14097) = 2.656$, $p < 0.001$. Difference between maximum and minimum firing rate = 1.526 Hz.
S6C	ANOVA statistics associated with the tuning curve: $F(47, 29517) = 3.293$, $p < 0.001$. Difference between maximum and minimum firing rate = 2.592 Hz.
S6D	ANOVA statistics associated with the tuning curve: $F(47, 29517) = 2.866$, $p < 0.001$. Difference between maximum and minimum firing rate = 1.824 Hz.
S6E	ANOVA statistics associated with the tuning curve: $F(62, 17087) = 3.292$, $p < 0.001$. Difference between maximum and minimum firing rate = 5.083 Hz.
S8B	Average firing rate within the significant time window (successful>unsuccessful) for successful trials: 0.307 Hz; average firing rate within the significant time window (successful>unsuccessful) for unsuccessful trials: 0.054 Hz; paired t test between successful and unsuccessful trials: $t(157) = 3.863$, $p < 0.001$. Average firing rate within the significant time window (successful>0) for successful trials: 0.354 Hz; one-sample t test for successful trials versus 0: $t(157) = 3.149$, $p = 0.002$.
S8D	Average firing rate within the significant time window for successful-unsuccessful trials in spatial cells: 0.252 Hz; average firing within the significant time window for successful-unsuccessful trials in non-spatial cells: 0.019 Hz; two-sample t test: $t(735) = 3.446$, $p = 0.001$.
S8F	Average firing rate within the significant time window (successful>unsuccessful) for successful trials: 0.194 Hz; average firing rate within the significant time window (successful>unsuccessful) for unsuccessful trials: -0.067 Hz; paired t test: $t(157) = 3.662$, $p < 0.001$. Average firing rate within the significant time window (successful>0) for successful trials: 0.248 Hz; one-sample t test for successful trials versus 0: $t(157) = 3.137$, $p = 0.002$.
S8H	Average firing rate within the significant time window for successful-unsuccessful trials in spatial cells: 0.267 Hz; average firing rate within the significant time window for successful-unsuccessful trials in non-spatial cells: -0.041 Hz; two-sample t test: $t(735) = 2.959$, $p = 0.003$.

The results in this table are for illustrative purposes only.

Table S3. Allocentric and egocentric single-neuron codes in the medial temporal lobe. Related to Figures 1 to 8.

	Allocentric		Egocentric	
	Animals	**Humans**	**Animals**	**Humans**
Cells with complex (or unknown) determinants of their receptive fields	Head-direction cell[a]	Direction cell[b,c]	Item-bearing cell[d]	Egocentric bearing cell[b]
	Place cell[e]	Place-like cell[b,f]	Item-bearing cell with distance tuning[d]	Egocentric bearing cell with distance tuning[b]
	Social place cell[g]	-	-	-
	Social place cell tuned to an inanimate object[g]	Spatial target cell[c]	Item-bearing cell[d]	-
	Grid cell[h]	Grid cell[i]	-	-
	Band cell[j]	-	-	-
	-	Path equivalence cell[k]	-	-
Cells with receptive fields determined by the environment's shape and geometry	Border cell[l]	-	-	-
	Boundary-vector cell[m]	-	Egocentric boundary cell[n]; item-bearing cell[d]	-
	-	-	Center-bearing cell[o]; item-bearing cell[d]	Egocentric bearing cell with a center reference point[b]; path cell[p]
	Spatial view cell[q]	-	Item-bearing cell[d]	Egocentric bearing cell with reference point at a boundary[b]
Cells with activity tuned to environmental content	Landmark-vector cell[r]; object-vector cell[s]; vector-trace cell[t]	-	Egocentric cue direction cell[u]; item-bearing cell[d]	Egocentric bearing cell with reference point at an object[b]
	-	-	Goal-vector cell[v]; item-bearing cell tuned to a goal[d]	-

[a](Taube et al., 1990); [b]this study; [c](Tsitsiklis et al., 2020); [d](Wang et al., 2018); [e](O'Keefe and Dostrovsky, 1971); [f](Ekstrom et al., 2003); [g](Omer et al., 2018); [h](Hafting et al., 2005); [i](Jacobs et al., 2013); [j](Krupic et al., 2012); [k](Miller et al., 2015); [l](Solstad et al., 2008); [m](Lever et al., 2009); [n](Hinman et al., 2019); [o](LaChance et al., 2019); [p](Jacobs et al., 2010); [q](Rolls, 1999); [r](Deshmukh and Knierim, 2013); [s](Høydal et al., 2019); [t](Poulter et al., 2020); [u](Wilber et al., 2014); [v](Sarel et al., 2017); the references are non-exhaustive; "-" denotes that no evidence has been obtained so far to the best of our knowledge.

Supplemental Figures

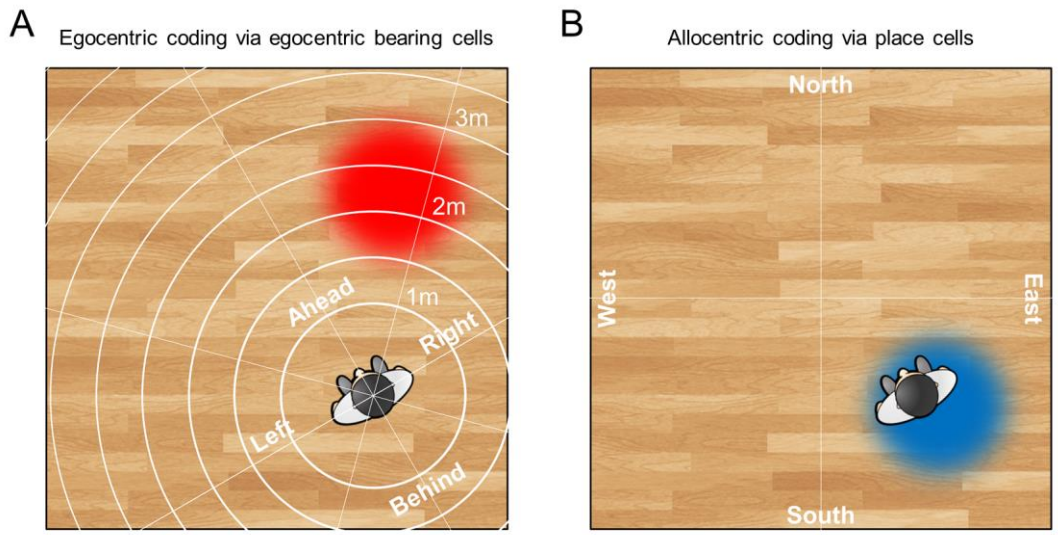

Figure S1. Illustration of the egocentric coding scheme of egocentric bearing cells as compared to the allocentric coding scheme of place cells. Related to Figures 2, 6, and S6. (**A**) Coding of spatial information in an egocentric reference frame (white lines), which is centered on the subject. The subject and the surrounding room are shown from a bird's eye view. The reference point of a hypothetical egocentric bearing cell is shown in red. The activity of this egocentric bearing cell provides the subject with the information that the area of the environment that is marked by the reference point is about 35° to the right and about 2 meters away from the subject. (**B**) Coding of spatial information in an allocentric reference frame, which is bound to the external environment. The place field of a hypothetical place cell is shown in blue. The activity of this place cell provides the subject with the information that the subject is standing in the south-east part of the environment.

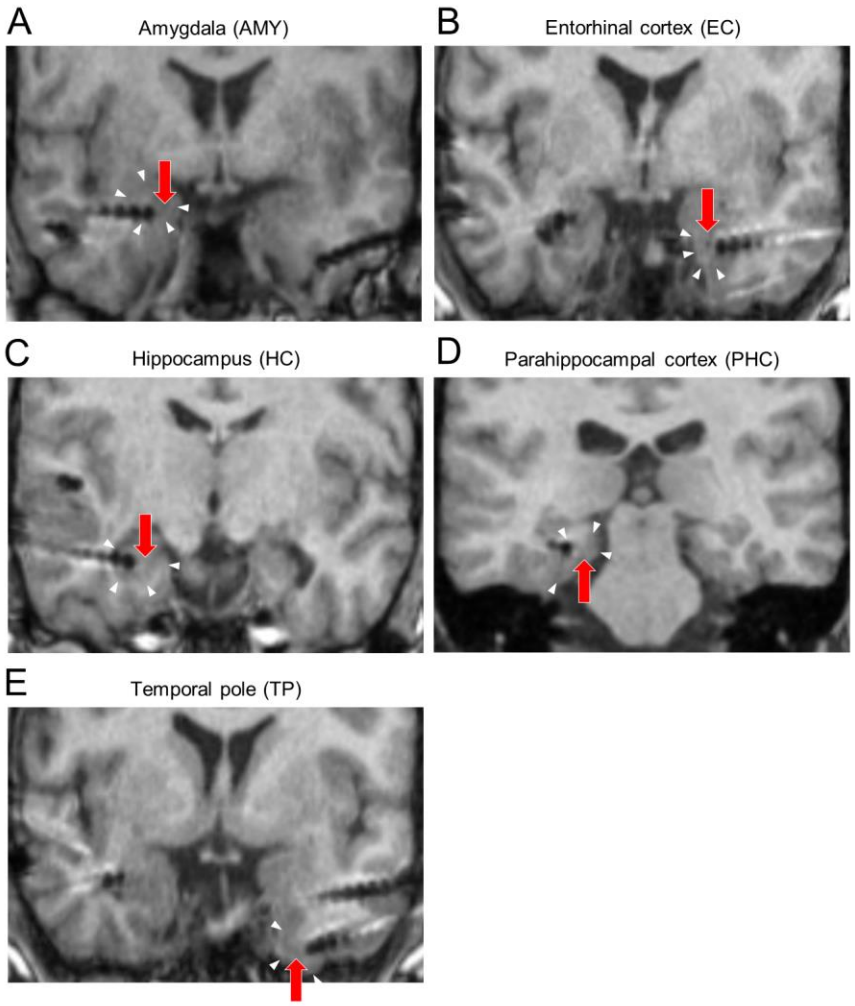

Figure S2. Examples of microelectrode locations. Related to Figures 2, 3, 4, and 6. (**A to E**) Example microelectrode locations in regions for which region-specific analyses were performed (i.e., amygdala, entorhinal cortex, hippocampus, parahippocampal cortex, and temporal pole). Electrode contacts of depth electrodes appear as dark circles on the MRI scans. Red arrows point at putative microelectrode locations, which protrude 3–5 mm from the tip of the depth electrode (often not visible on MRI scans). White triangles indicate the borders of the different brain regions.

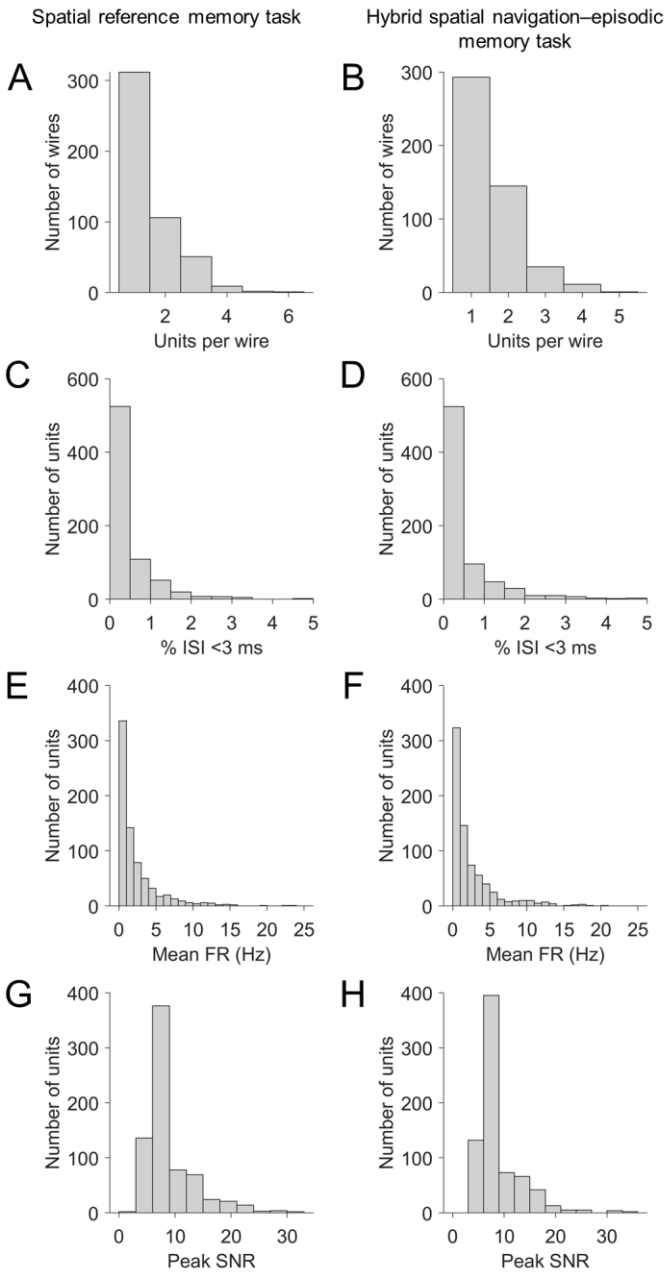

Figure S3. Quality assessment of single-neuron recordings. Related to Figures 2 to 8. (**A and B**) Histogram of units per wire. On average, 1.516 ± 0.037 [1.520 ± 0.034 (mean ± SEM)] units per wire were recorded. (**C and D**) Histogram of the percentages of inter-spike intervals (ISIs) that were shorter than 3 ms. On average, units exhibited 0.434 ± 0.031% [0.545 ± 0.040% (mean ± SEM)] ISIs that were shorter than 3 ms. There was 1 unit [5 units] with values >5%. (**E and F**) Histogram of mean firing rates (FRs). On average, units exhibited mean FRs of 2.268 ± 0.112 [2.437 ± 0.115 (mean ± SEM)] Hz. (**G and H**) Histogram of the mean waveform peak signal-to-noise ratio (SNR) of each unit. On average, the SNR of the mean waveform peak was 8.820 ± 0.168 [8.704 ± 0.164 (mean ± SEM)]. Numbers outside brackets refer to the spatial reference memory task (panels **A**, **C**, **E**, and **G**); numbers inside brackets refer to the hybrid spatial navigation–episodic memory task (panels **B**, **D**, **F**, and **H**).

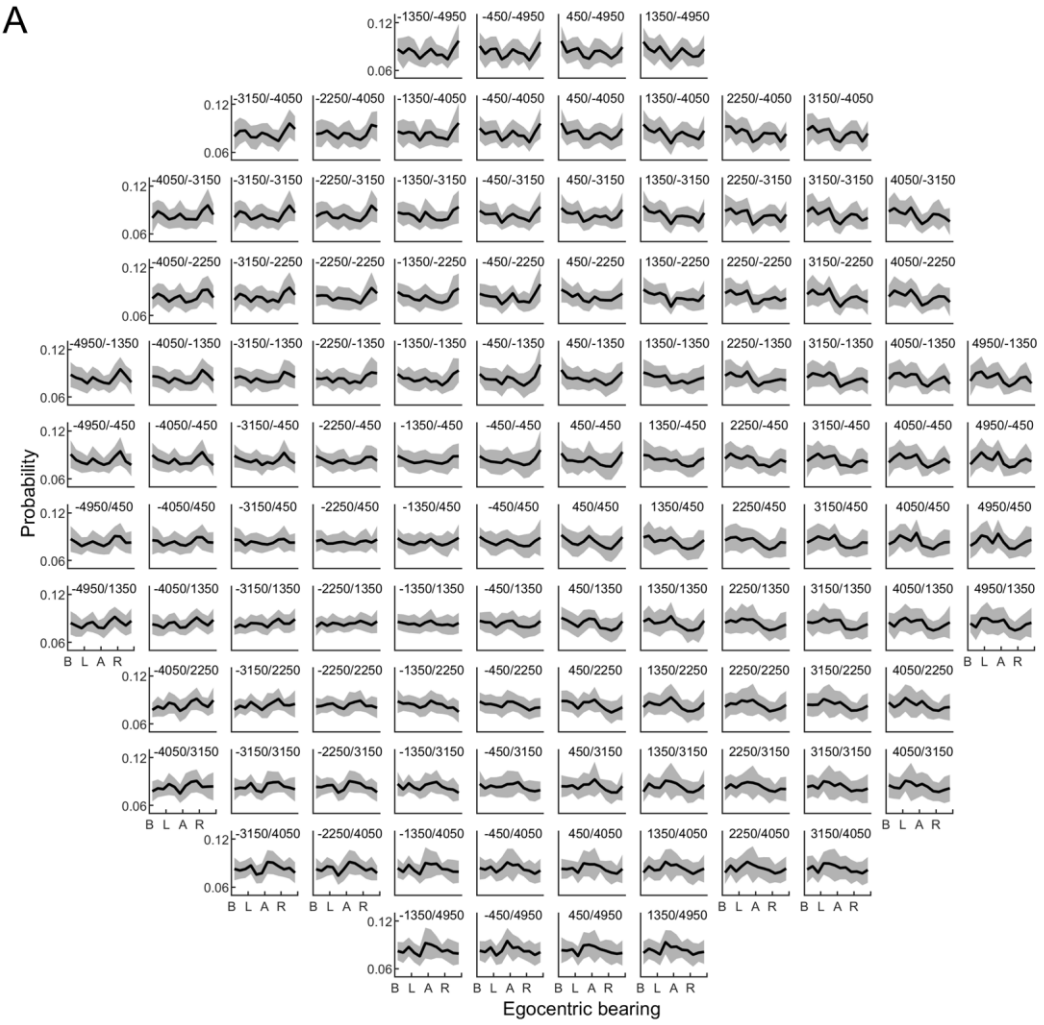
A
Probability
0.12
0.06
-1350/-4950
-450/-4950
450/-4950
1350/-4950
-3150/-4050
-2250/-4050
-1350/-4050
-450/-4050
450/-4050
1350/-4050
2250/-4050
3150/-4050
-4050/-3150
-3150/-3150
-2250/-3150
-1350/-3150
-450/-3150
450/-3150
1350/-3150
2250/-3150
3150/-3150
4050/-3150
-4050/-2250
-3150/-2250
-2250/-2250
-1350/-2250
-450/-2250
450/-2250
1350/-2250
2250/-2250
3150/-2250
4050/-2250
-4950/-1350
-4050/-1350
-3150/-1350
-2250/-1350
-1350/-1350
-450/-1350
450/-1350
1350/-1350
2250/-1350
3150/-1350
4050/-1350
4950/-1350
-4950/-450
-4050/-450
-3150/-450
-2250/-450
-1350/-450
-450/-450
450/-450
1350/-450
2250/-450
3150/-450
4050/-450
4950/-450
-4950/450
-4050/450
-3150/450
-2250/450
-1350/450
-450/450
450/450
1350/450
2250/450
3150/450
4050/450
4950/450
-4950/1350
-4050/1350
-3150/1350
-2250/1350
-1350/1350
-450/1350
450/1350
1350/1350
2250/1350
3150/1350
4050/1350
4950/1350
-4050/2250
-3150/2250
-2250/2250
-1350/2250
-450/2250
450/2250
1350/2250
2250/2250
3150/2250
4050/2250
-4050/3150
-3150/3150
-2250/3150
-1350/3150
-450/3150
450/3150
1350/3150
2250/3150
3150/3150
4050/3150
-3150/4050
-2250/4050
-1350/4050
-450/4050
450/4050
1350/4050
2250/4050
3150/4050
-1350/4950
-450/4950
450/4950
1350/4950
B L A R
Egocentric bearing

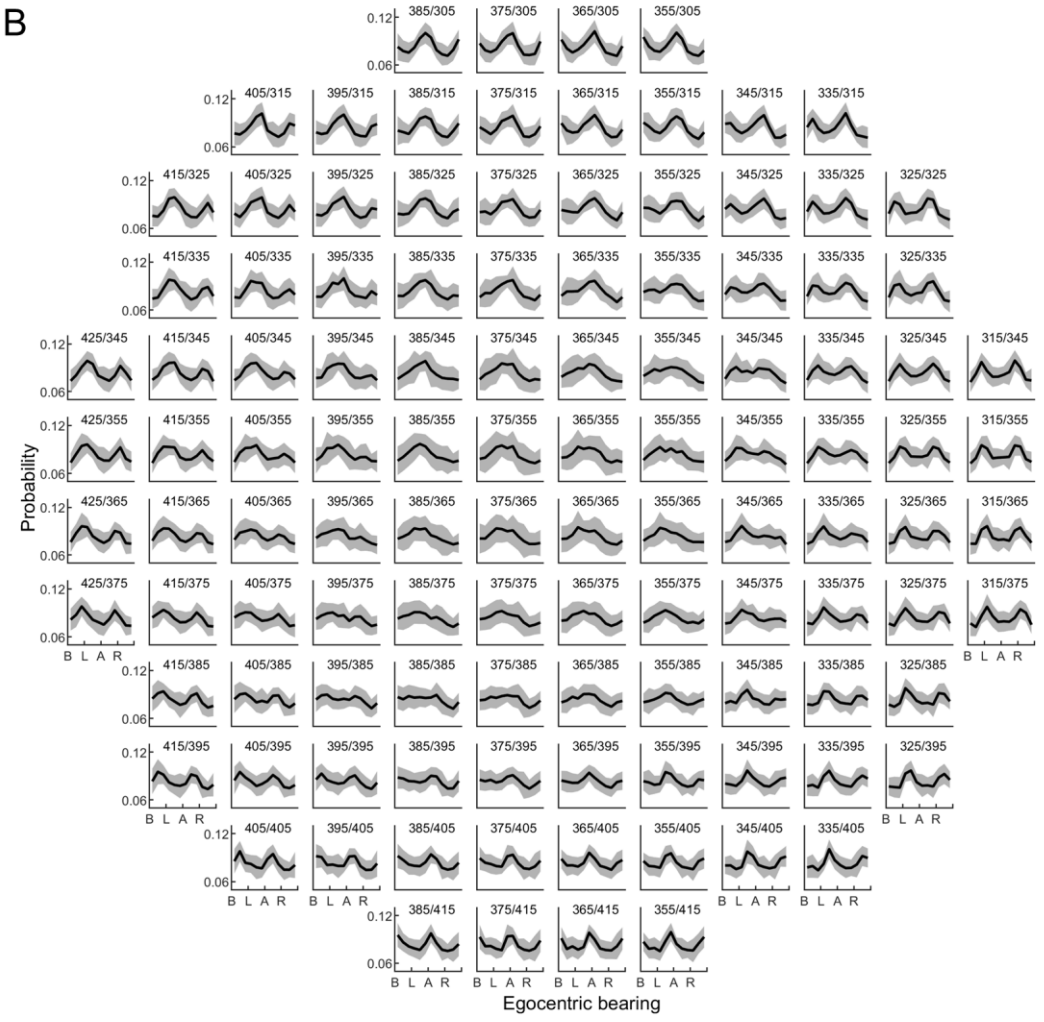
B
Probability
0.12
0.06
385/305
375/305
365/305
355/305
405/315
395/315
385/315
375/315
365/315
355/315
345/315
335/315
415/325
405/325
395/325
385/325
375/325
365/325
355/325
345/325
335/325
325/325
415/335
405/335
395/335
385/335
375/335
365/335
355/335
345/335
335/335
325/335
425/345
415/345
405/345
395/345
385/345
375/345
365/345
355/345
345/345
335/345
325/345
315/345
425/355
415/355
405/355
395/355
385/355
375/355
365/355
355/355
345/355
335/355
325/355
315/355
425/365
415/365
405/365
395/365
385/365
375/365
365/365
355/365
345/365
335/365
325/365
315/365
425/375
415/375
405/375
395/375
385/375
375/375
365/375
355/375
345/375
335/375
325/375
315/375
415/385
405/385
395/385
385/385
375/385
365/385
355/385
345/385
335/385
325/385
415/395
405/395
395/395
385/395
375/395
365/395
355/395
345/395
335/395
325/395
405/405
395/405
385/405
375/405
365/405
355/405
345/405
335/405
385/415
375/415
365/415
355/415
B L A R
Egocentric bearing

Figure S4. Behavioral sampling of egocentric bearing towards candidate reference points. Related to Figures 2, 3, 6, and 7. For each candidate reference point, the distribution of egocentric bearings towards this candidate point is depicted. (**A**) Data from the spatial reference memory task; (**B**) data from the hybrid spatial navigation–episodic memory task. Distributions are expressed as probabilities. Black line, mean across sessions; gray area, SD across sessions. Numbers above each subpanel indicate the (x/y) or (x/z)-coordinate of the candidate reference point in virtual units. A (B; L; R), ahead (behind; to the left; to the right) of the subject.

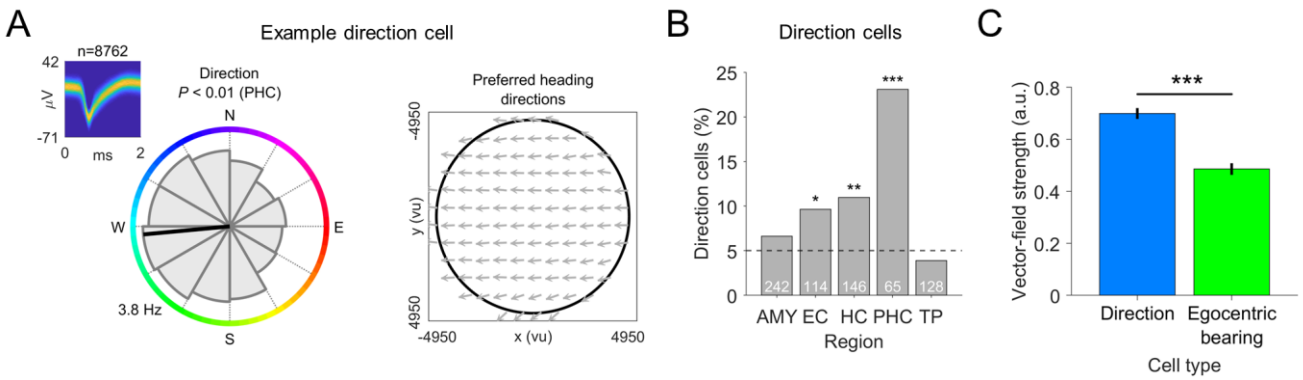

Figure S5. Direction cells in the spatial reference memory task. Related to Figure 3. (**A**) Left, example direction cell encoding allocentric direction. Gray shaded area, tuning curve; black line, preferred direction; colored circle, allocentric direction. p value results from the comparison against surrogate statistics. Right, vector-field map of this example direction cell, illustrating that allocentric direction tuning is similar across the environment. Black circle, environmental boundary. (**B**) Distribution of allocentric direction cells (n = 78) across brain regions. Dashed line, 5% chance level. White numbers, total number of cells per region. (**C**) Comparison of vector-field strengths between direction cells and egocentric bearing cells. Error bars indicate SEM. AMY, amygdala; EC, entorhinal cortex; HC, hippocampus; PHC, parahippocampal cortex; TP, temporal pole. E, east; N, north; S, south; W, west. a.u., arbitrary units; ms, milliseconds; μV, microvolts; vu, virtual units. *p < 0.05; **p < 0.01; ***p < 0.001.

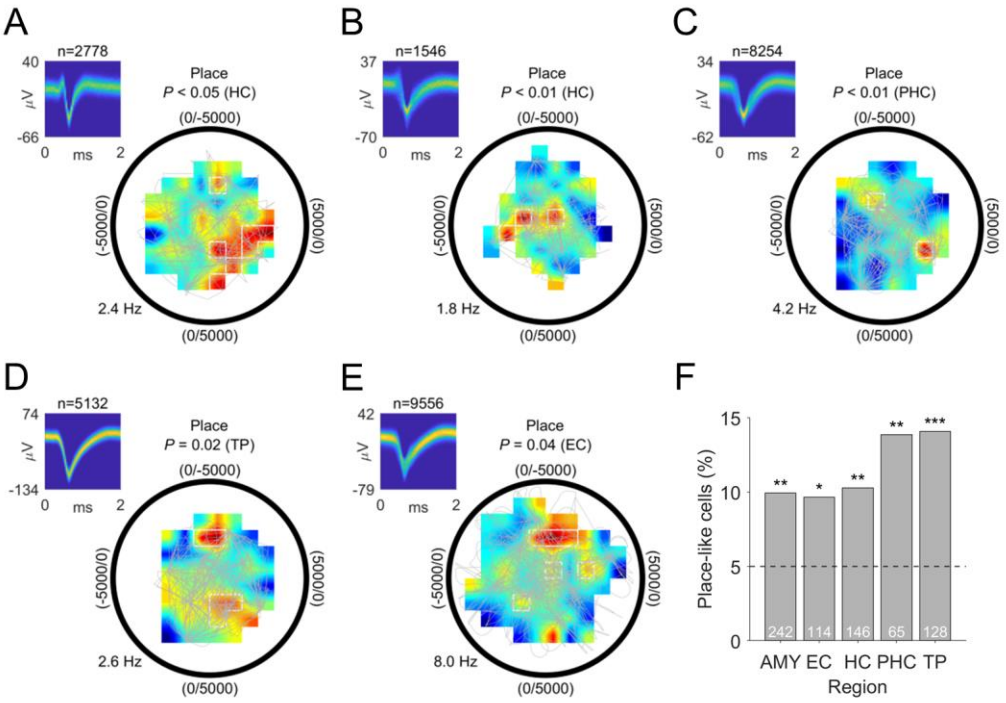

Figure S6. Place-like cells in the spatial reference memory task. Related to Figure 3. (**A to E**) Examples of place-like cells. For example, the hippocampal place-like cell shown in (**A**) increased its firing rate when the subject was in the "southeast" part of the environment. Colored areas depict smoothed firing rates as a function of place (dark blue, low firing rate; dark red, high firing rate). White line delineates place bins. Gray line, patient's navigation path. Only bins with ≥5 separate traversals were included in the analysis to ensure sufficient behavioral sampling. p values result from the comparison against surrogate statistics. Black circle, environmental boundary. ms, milliseconds; μV, microvolts. (**F**) Distribution of place-like cells across brain regions (n = 85; binomial test vs. 5% chance, $p < 0.001$). Dashed line, 5% chance level. White numbers, total number of cells per region. AMY, amygdala; EC, entorhinal cortex; HC, hippocampus; PHC, parahippocampal cortex; TP, temporal pole. *$p < 0.05$; **$p < 0.01$; ***$p < 0.001$.

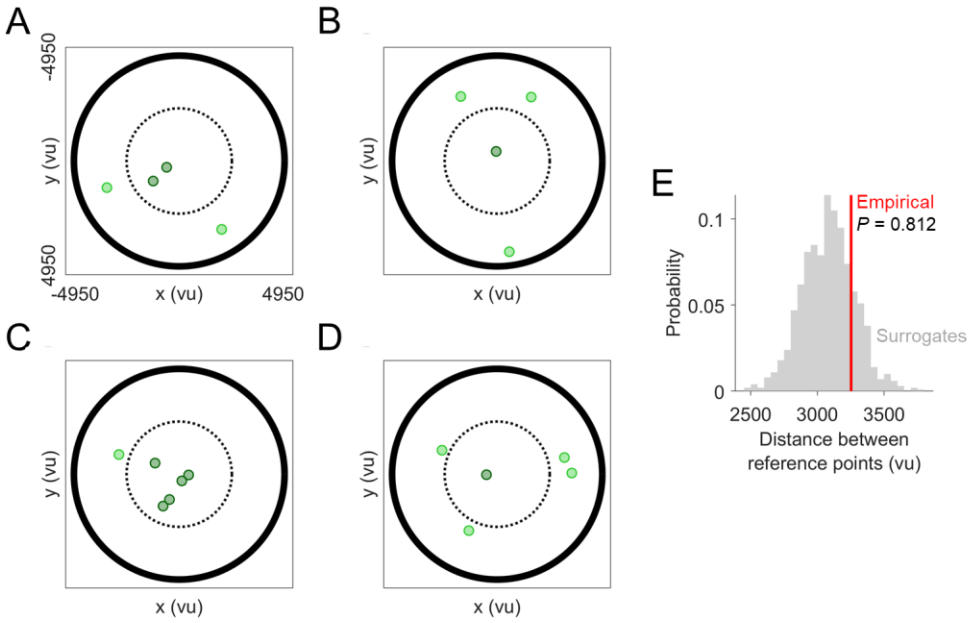

Figure S7. Session-wise examples of reference-point distributions in the spatial reference memory task. Related to Figure 3. (**A to D**) Examples of the spatial distribution of reference points in four different sessions. There were both sessions in which the reference points appeared randomly distributed across the environment (e.g., panel **B**) and sessions in which the reference points appeared relatively close to each other (e.g., panel **C**). Dark green dots, center reference points; lime green dots, periphery reference points; solid black line, environmental boundary; dotted black line, radius separating center reference points from periphery reference points. (**E**) Evaluation of the distance between reference points from the same session ("Empirical") versus the distance between reference points from different sessions ("Surrogates"), showing that reference points from the same session were not closer to each other than reference points from different sessions. vu, virtual units.

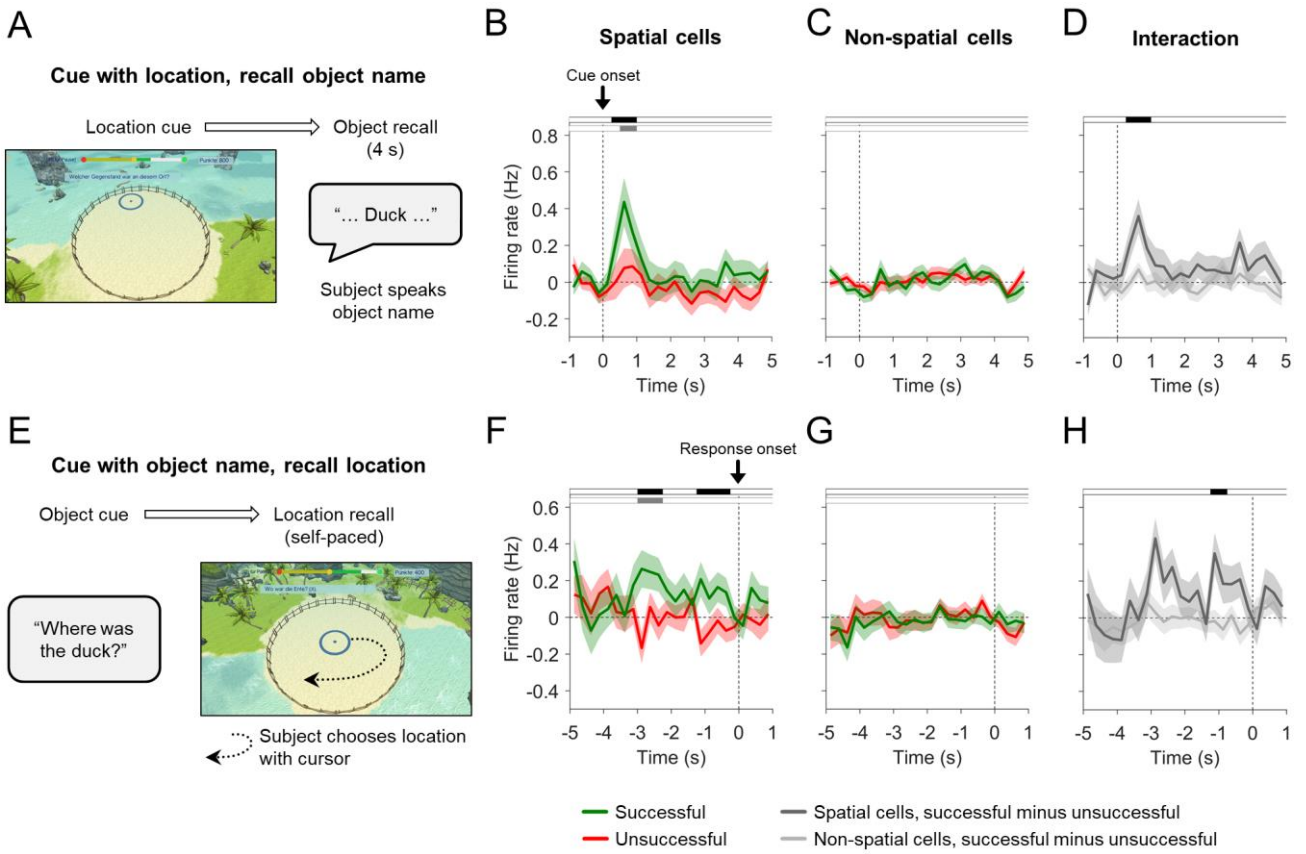

Figure S8. Spatial cells activate during successful episodic memory recall. Related to Figure 8. (**A**) Schematic for location-cued object recall. (**B and C**) Firing rates of spatial cells (**B**) and non-spatial cells (**C**) during successful (green) versus unsuccessful (red) object recall. Spatial cells exhibited increased firing rates during successful object recalls shortly after the location cue (cluster-based permutation test for successful vs. unsuccessful recall periods, $p = 0.004$; cluster-based permutation test for successful recall periods vs. 0, $p = 0.023$). Spatial cells comprise egocentric bearing cells, direction cells, and place-like cells; non-spatial cells comprise all other cells. (**D**) Interaction effect showing a significant difference between the activity of spatial cells (dark gray) and non-spatial cells (light gray) during successful versus unsuccessful recall periods (cluster-based permutation test for an interaction between "performance" and "cell type", $p = 0.011$). (**E**) Schematic for object-cued location recall. (**F and G**) Response-locked firing rates of spatial cells (**F**) and non-spatial cells (**G**) during successful (green) versus unsuccessful (red) location recall. Spatial cells exhibited increased firing rates during successful location recalls (cluster-based permutation test for successful vs. unsuccessful recall periods, $p = 0.007$ and $p = 0.010$, respectively; cluster-based permutation test for successful recall periods vs. 0, $p = 0.004$). (**H**) Interaction effect showing a significant difference between the activity of spatial cells (dark gray) and non-spatial cells (light gray) during successful versus unsuccessful recall periods (cluster-based permutation test for an interaction between "performance" and "cell type", $p = 0.035$). Firing rates in **B**, **C**, **D**, **F**, **G**, and **H** are baseline-corrected with respect to a one-second baseline interval before the onset of the recall period. Shaded areas, SEM across cells. In **B**, **C**, **F**, and **G**, black shadings at top indicate significant clusters of firing-rate differences between successful and unsuccessful recall periods; gray shadings indicate significant deviations of firing rates from 0 during successful recall periods (cluster-based permutation tests, $p < 0.05$). In **D** and **H**, black shadings at top indicate significant interaction effects (cluster-based permutation tests, $p < 0.05$). All cluster-based permutation tests control for multiple comparisons across the entire depicted time window.